Liquid-metal-jet anode x-ray tube

Oscar Hemberg, MEMBER SPIE
Mikael Otendal, MEMBER SPIE
Hans M. Hertz, MEMBER SPIE
Royal Institute of Technology
Department of Physics
Biomedical and X-Ray Physics
SE-10691 Stockholm, Sweden
E-mail: oscar.hemberg@biox.kth.se

Abstract. We describe a novel electron-impact x-ray source based on a high-speed liquid-metal-jet anode. Thermal power load calculations indicate that this new anode concept potentially could increase the achievable brightness in compact electron-impact x-ray sources by more than a factor 100 compared to current state-of-the-art rotating-anode or microfocus sources. A first, successful, low-power proof-of-principle experiment is described and the feasibility of scaling to high-brightness and high-power operation is discussed. Some possible applications that would benefit from such an increase in brightness are also briefly described.
[DOI: 10.1117/1.1737787]

Subject terms: brightness; x-ray source; electron-impact; liquid-metal jet.

Paper 030429 received Sep. 2, 2003; revised manuscript received Oct. 24, 2003; accepted for publication Jan. 12, 2004. This paper is a revision of a paper presented at the SPIE conference on Laser-Generated and other Laboratory X-Ray and EUV Sources, Optics, and Applications, August 2003, San Diego, Calif. The paper presented there appears (unrefereed) in SPIE Proceedings Vol. 5196.

1 Introduction

X rays have been used for imaging ever since their discovery by Roentgen at the turn of the 19th century. Since the available x-ray optics is severely limited, x-ray imaging is still mostly based on absorption shadowgraphs. This is basically true even for modern computer tomography (CT) imaging and, as a consequence, the brightness of the x-ray source is the key figure of merit, limiting both the exposure time and the attainable resolution in many applications.

Today x-ray imaging is a widespread and standard method in science, medicine, and industry. Although well established, there are numerous applications that would greatly benefit from an increased brightness. Among these are applications in medicine requiring high spatial resolution,[1–3] such as mammography and angiography, and emerging techniques requiring monochromatic radiation,[4] which currently cannot be achieved with reasonable exposure times. Also, certain protein crystallography,[5] today only possible at synchrotron radiation facilities, may be feasible with a compact source. Furthermore, a significant increase in the brightness of compact x-ray sources could enable phase imaging with reasonable exposure times.[6] This is important since the phase contrast is often much higher than the absorption contrast. In addition, phase contrast imaging could reduce the absorbed dose during imaging.

The basic physics in x-ray production in compact electron-impact sources has not changed since the days of Roentgen. As the electrons impact the target they lose energy in one of two ways: either they can be decelerated in the electric field close to an atomic nucleus and emit continuous bremsstrahlung radiation, or they can knock out an innershell electron, resulting in the emission of a characteristic x-ray photon when the vacancy is filled. The efficiency of x-ray production by electron impact is very poor, typically below 1%, and the bulk of the energy carried by the electron beam is converted to heat.[7]

1.1 *Current State-of-the-Art Sources*

The brightness of current state-of-the-art compact electron-impact x-ray sources is limited by thermal effects in the anode. The x-ray brightness [i.e., photons/(mm^2 sr s bandwidth)] is proportional to the effective electron-beam power density at the anode, which must be limited not to melt or otherwise damage the anode. Since the first cathode-ray tubes only two fundamental techniques, the line focus and the rotating anode, have been introduced to improve the power load capacity of the anode. These are illustrated in Fig. 1.

The line focus principle, introduced in the 1920s, utilizes the fact that the x-ray emission is non-Lambertian to increase the effective power load capacity by extending the targeted area but keeping the apparent source area almost constant by viewing the anode at an angle. Ignoring the Heel effect and field of view, this trick increases the attainable power load capability up to $\sim 10\times$. The rotating anode was introduced in the 1930s to further extend the effective electron-beam-heated area by rotating a cone-shaped anode to continuously provide a cool target surface.

After these improvements, progress as regards brightness has been rather slow for compact electron-impact sources and has only been due to engineering perfection in terms of target material, heat conduction, heat storage, speed of rotation, etc. Current state-of-the-art sources now allow for 100 to 150 kW/mm^2 effective electron-beam power density. Typical high-end implementations are, e.g., 10 kW, 0.3×0.3 mm^2 effective x-ray spot size angiography systems and 1.5 kW, 0.1×0.1 mm^2 effective x-ray spot size fine-focus mammography systems. Low-power microfocus sources (see, e.g., Ref. 8; 4 W, 5 μm effective x-ray spot

 0091-3286/2004/$15.00

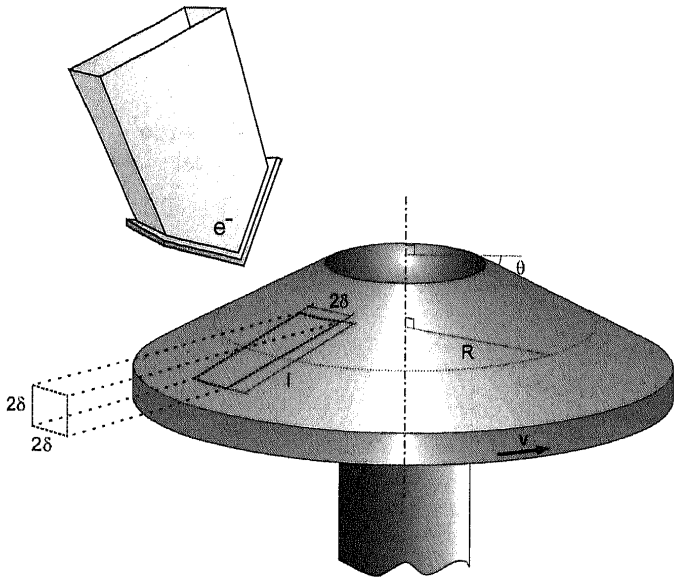

Fig. 1 Schematic view of a rotating-anode source.

diameter) have similar effective power densities (200 kW/mm^2) and are also limited by thermal effects.

The power load limit of a modern rotating anode can be calculated by[2]

$$\frac{P}{A_{\text{effective}}}=\frac{\pi l(T_{\max}-\Delta T_{\text{margin}}-T_{\text{base}})(\lambda\rho c_p f R\delta)^{1/2}}{4\delta^2\{1+k(tf\delta/\pi R)^{1/2}\}}, \quad (1)$$

where $A_{\text{effective}}$ is the apparent x-ray source area, R is the anode radius, l is the spot height, 2δ is the spot width, $T_{\max}$ is the maximum permissible temperature before breakdown, ΔT_{margin} is a safety margin, T_{base} is the anode starting temperature, λ is the thermal conductivity, ρ is the density, c_p is the specific heat capacity, f is the rotation frequency, t is the load period, and k is a correction factor taking into account radial heat conduction, heat loss by radiation, and anode thickness. As can be seen from Eq. (1), the only way to increase the power load limit is to increase the spot speed, i.e., f and R. Unfortunately even a quite unrealistic set of parameters (1-m-diam anode and 1-kHz rotation) would only increase[4] the output ~6×. It therefore seems unlikely that conventional x-ray source technology can be developed much further, even with significant engineering efforts.

A way to increase the brightness in compact electron-impact-based hard x-ray sources would be a fundamentally different anode configuration enabling a higher electron-beam power density. In this paper, we report on the status of a new liquid-metal-jet anode concept.[9] As will be shown in the following, this anode configuration could enable a significantly higher (>100×) thermal load per area than current state of the art due to fundamentally different thermal limitations. In brief, higher speed accounts for one order of magnitude and a higher heat capacity for another order of magnitude. Liquid-jet systems have been extensively used as targets in negligible-debris laser-produced plasma soft x-ray and EUV sources.[10–12] A liquid-gallium jet has also been used as target in hard x-ray production in femtosecond laser-plasma experiments.[13] Furthermore, an electron beam has been combined with a water jet for low power soft x-ray generation via fluorescence.[14] X-ray tubes with liquid anodes, either stationary or flowing over surfaces, have previously been reported,[15,16] but their advantages for high-brightness operation are limited due to the intrinsically low flow speed and cooling capacity of such systems. Recent work also includes a liquid anode flowing behind a thin window.[17]

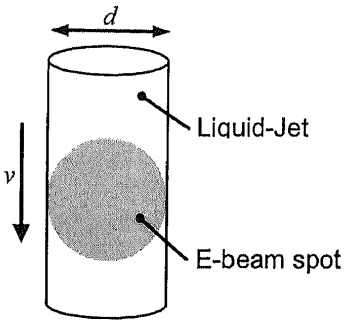

Fig. 2 Schematic view of the liquid-metal-anode concept. In its simplest form, a liquid-metal jet with a diameter d and speed v is targeted with an electron beam with matching focus size.

2 Liquid-Metal-Jet Anode

A schematic view of the liquid-metal-jet-anode electron-impact hard x-ray tube is shown in Fig. 2. A thin (<100 μm diameter) high-speed (>50 m/s) liquid-metal jet is injected into vacuum and targeted by a focused electron beam.

2.1 *Material Selection*

There are a number of criteria for material selection for the liquid-jet anode. First, it is vital that the material is electrically conductive to transport the current carried by the electron beam to avoid charging and subsequent repulsion. Furthermore, it is desirable with a low-vapor-pressure material to simplify vacuum operation. For efficient x-ray production it is also favorable with a high-Z material with appropriate line emission. These requirements make metals with fairly low melting point good candidates. Normally, an elementally pure liquid is preferred since it will produce a "clean" x-ray spectrum, but alloys could be interesting due to different thermal and fluid dynamic properties, or, conceivably, if a certain spectral distribution of x-ray energies is desired. Also, it is preferable with materials that are not prone to oxidization or are otherwise reactive or harmful.

2.2 *Power Load Calculations*

The power required to evaporate a liquid-metal jet (as shown in Fig. 2) is, given by

$$P=\frac{\pi d^2}{4}v\rho(\Delta T c_p+E_{\text{vap}}), \quad (2)$$

where d is the jet diameter, v is the jet speed, ρ is the density, ΔT is the temperature span from initial jet temperature to boiling temperature ($\Delta T\approx T_{\text{boil}}-T_{\text{melt}}$), c_p is the specific heat capacity, and E_{vap} is the heat of vaporization. This result omits heat transfer by conduction or radia-

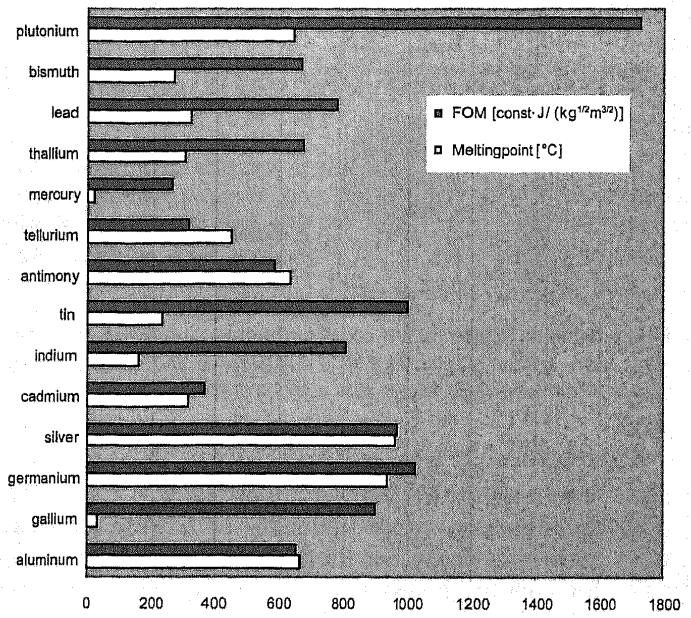

Fig. 3 Diagram showing FOM and melting point of different materials. The FOM is scaled so that Sn is 1000. The attainable brightness scales linearly with this number as seen in Eqs. (4) and (6).

tion and is, thus, a minimum-power scenario. Given a certain backing pressure p on the liquid, the jet speed is given by[18]

$$v=\sqrt{\frac{2p}{\rho}}. \tag{3}$$

Combining Eqs. (2) and (3) and assuming a circular electron beam focus with the same diameter as the liquid jet d, the maximum electron-beam power density on the liquid-metal jet can be expressed as

$$\frac{P}{A}=\sqrt{2p\rho}(\Delta Tc_p+E_{\text{vap}}). \tag{4}$$

The theoretical bremsstrahlung yield for a thick target is given by[7]

$$\eta=9.2\times 10^{-10}ZV, \tag{5}$$

where Z is the atomic number, and V is the acceleration voltage. Multiplying Eqs. (4) and (5), and keeping only the material specific parameters, a figure of merit (FOM) can be calculated according to

$$\text{FOM}=Z\sqrt{\rho}(\Delta Tc_p+E_{\text{vap}}). \tag{6}$$

As already mentioned the line emission and the vapor pressure are also important, but as a first approximation this FOM is useful for selecting an appropriate anode material.

Figure 3 shows the melting points and the FOMs for a range of possible materials. Although not included in the FOM, a low melting point is, purely from an engineering perspective, an advantage. As is clear from the diagram, Sn is a good choice, especially for applications matched to its 25-keV line emission. Furthermore, it has a low vapor pressure and a low melting point and is readily available and not very toxic or reactive.

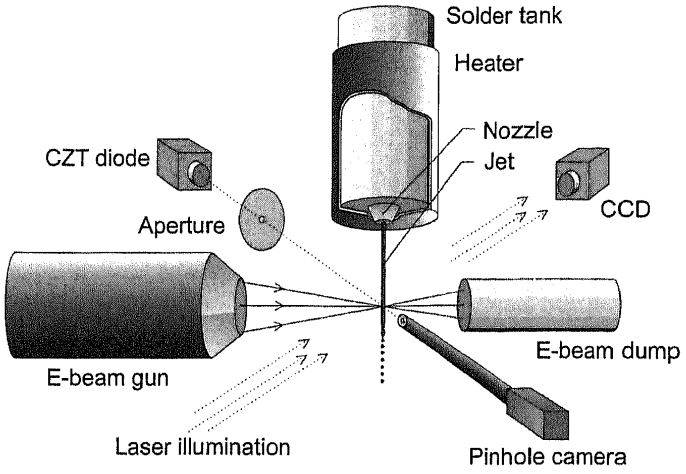

Fig. 4 Schematic view of the proof-of-principle liquid-metal-jet anode electron-impact x-ray source experimental arrangement.

3 Experimental Arrangement

This new liquid-metal-jet anode has been demonstrated in a first low-power proof-of-principle experiment.[9] For this experiment a Sn63Pb37 solder alloy (mp 183 °C) was used for its low melting point, good availability, and high Sn content. The proof-of-principle experimental arrangement basically consists of a liquid-solder system, an electron beam, and diagnostics equipment. The electron beam is focused on the liquid-solder jet and the entire system is pumped by a 500 l/s turbo-drag pump, keeping the pressure at $\sim 10^{-5}$ mbar during operation. The spent liquid is simply collected in a container in the bottom of the vacuum chamber. The arrangement is shown in Fig. 4 and each of the different subsystems are described in the following.

3.1 *Liquid-Metal-Jet System*

The base of the liquid-metal-jet system is a 0.15-l high-pressure tank enclosed in an IR heater and filled with liquid solder. The heater is a low-current design using counteracting magnetic fields to minimize the magnetic leak field that could otherwise perturb the electron beam. The entire assembly is grounded and use of insulators minimized to prevent local charge build-up. The nozzle is a 75- or 50-μm ruby pin hole with an integrated stainless steel particle filter. A nitrogen backing pressure of up to 200 bar is applied, resulting in a jet speed of up to ~60 m/s. At maximum jet speed the entire solder tank is emptied in ~10 min. Fortunately, a stable jet can normally be operated with low backing pressure (<5 bar) and the experimental time can then be extended to hours.

The liquid jet is characterized by a flash photography system using a 12× zoom microscope to image the jet, back illuminated by a 4-ns pulsed frequency-doubled Nd:YAG laser. This was used both to characterize the positional stability of the liquid jet, as well as the hydrodynamics of the jet by studying the jet breakup. Figure 5 shows a typical jet image and the jet stability was measured to better than 5

Fig. 5 Flash photograph (4 ns exposure time) of a ~50 μm, ~35 m/s liquid-solder jet showing the ordered Rayleigh droplet breakup characteristic of laminar flow. Scale bar is 5 mm.

μm, 10 mm from the nozzle orifice. The hydrodynamics of liquid-metal jets in vacuum are briefly discussed in Sec. 6.2.

3.2 *Electron-Beam System*

The current electron-beam system performance is ~100 W (50 kV and 2 mA) continuously into a ~150 μm FWHM diameter spot at a working distance of ~10 cm. The low-perveance design[19] is source limited, and based on a 1.78-mm-diam flat single crystal LaB_6 thermionic emitter. The 50-kV acceleration field is almost flat between the cathode and grounded anode, with the anode exit aperture acting as a negative lens. The virtual point source produced by the aperture is then imaged by an electromagnetic lens. The anode aperture and the lens exit aperture are small enough to efficiently maintain a pressure difference as the electron gun system is pumped by its own 250 l/s turbo-drag pump. The pressure during operation is lower than 10^{-7} mbar, as required by the cathode, even when the main chamber vacuum is in the 10^{-4} to 10^{-5} mbar range. The focal point can be shifted several millimeters in any direction by adjusting the lens focal strength and using deflection coils for beam steering.

3.3 *X-Ray Spectroscopy*

Spectral characterization of the source is made with a commercial CdZnTe (CZT) diode system (Amptek XR-100T-CdZnTe). The efficiency in the interesting spectral range (7 to 50 keV) is good (>90%) and calibrated. Unfortunately, the maximum count rate is only ~10^4 counts/s, which means that the source must be attenuated if operated at high power. X-ray-attenuation filters are not unproblematic, and the system instead uses thick tungsten pinhole apertures to attenuate the source without perturbing the spectra. Unfortunately, very-high aspect-ratio holes (1:40) must be used when measuring the spectra at full power. To avoid possible alignment errors the calibrated spectra have been recorded using a 1:2 aspect ratio hole in combination with a low beam current to limit the count rate.

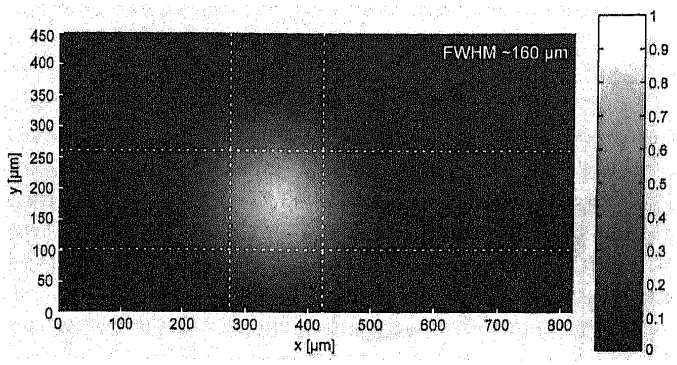

Fig. 6 Pinhole image of the x-ray spot produced on the beam dump for measuring size and stability. Electron-beam power is ~100 W and working distance is ~10 cm.

3.4 *X-Ray Pinhole Camera*

To measure the x-ray spot size a CCD-based (X-Ray FDI from Photonic Science) pinhole camera is used. The resolution in a pinhole camera is, when as a first approximation ignoring the diffraction term, given by pinhole diameter. With the ~150 μm electron-beam spot size, a 50-μm tungsten pinhole is sufficient in the camera. The pinhole material must be rather thick to reduce the background noise and the 1:20 aspect ratio pinhole requires careful prealignment. The required exposure time is small enough for real-time viewing of the x-ray spot even at modest electron-beam current, and can be used to fine-tune the electron-beam settings for maximum power density.

4 Results

Figure 6 shows an x-ray pinhole-camera image of x-ray spot produced by the 100-W electron beam when focused onto the beam dump. The FWHM of the spot is ~150 μm, a number that is independent of beam power within the measurement range (10 to 100 W). Figure 7 shows an image of a ~75-μm, ~50-m/s liquid-solder jet targeted by the ~100-W, ~150-μm FWHM electron beam. When operating a low-speed jet and the 100-W electron beam, a thermal glow is visible and evaporation and boiling phe-

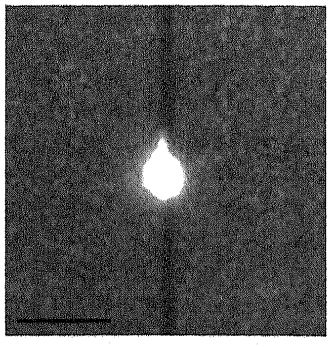

Fig. 7 Photograph of a ~75-μm, ~50-m/s solder-jet targeted by a ~100-W, ~150-μm FWHM electron beam. Scale bar is 0.5 mm.

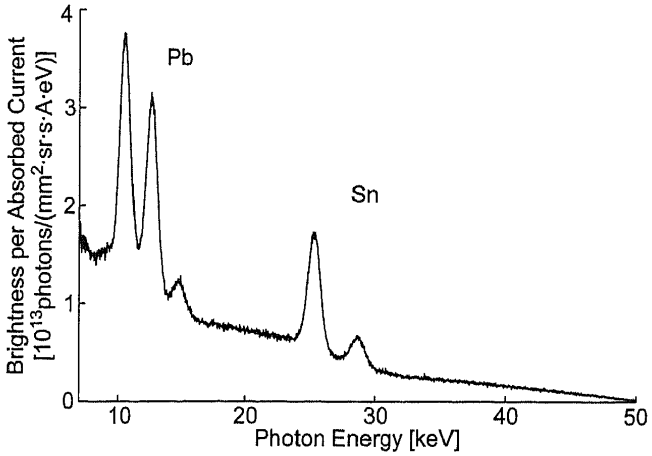

Fig. 8 X-ray spectrum obtained in the proof-of-principle liquid-metal-jet anode electron-impact x-ray-source experiment. As expected, the spectra shows Pb *L*-lines and Sn *K*-lines on top of the continuous bremsstrahlung background. The spectrum was recorded at an 90-deg angle with respect both to the electron beam and the liquid-solder jet.

nomena can be observed. This is in accordance with the power-load-limit calculations in Sec. 2.2. In some instances, the electron-beam can induce droplet breakup downstream of the interaction point not present when the electron beam was turned off.

As previously stated, the spectrum was recorded at a low electron-beam current (8.3 ± 0.4 μA absorbed by the jet, 1 W total beam power). The absorbed current was measured as the difference in collected beam-dump current with and without the liquid-solder jet in the focus. The jet absorbed 42% of the total electron-beam current. Assuming a ~ 75-μm diameter jet and a Gaussian electron-beam spot this corresponds to an electron-beam FWHM of ~ 150 μm, which is in good agreement with the pinhole measurements already discussed. Thus, the resulting x-ray spot size is assumed to be a ~ 75-μm-wide center cutout (corresponding to the jet diameter) of the incident electron-beam spot, but no x-ray image has yet been recorded to verify this.

The spectrum in Fig. 8 has been corrected for detector efficiency, vacuum-window absorption, measurement geometry, x-ray-source size, and absorbed current. The major uncertainty is in the source size and angular distribution (here simply assumed to be uniform over 4π sr). The brightness data is estimated to be correct within $\pm 50\%$ in the measurement direction. The theoretical bremsstrahlung yield above 7 keV for a traditional solid anode is 0.20% for Sn and 0.32% for Pb. Integrating the spectrum (not including the line-emission peaks) in Fig. 8, the total bremsstrahlung efficiency is 0.19%. The difference is believed to be partly due to geometrical effects. Finally, we estimated the maximum brightness achieved in the proof-of-principle experiment. Given that the x-ray flux is proportional to the absorbed electron-beam power and that the e-beam focusing is independent of power, the Sn K_α-line brightness is 1.4×10^{10} photons/(mm^2 sr s eV). The number corresponds to 100-W operation and a 42% absorption ratio resulting in a power density of ~ 3 kW/mm^2 within the FWHM of the spot.

5 Near-Term Improvements

The near-term goals of the project are to upgrade the source in two respects. The electron-beam system will be upgraded to its original design specifications of 500 W into < 100 μm. The focal-spot electron-beam power density will then be ~ 100 kW/mm^2, i.e., in parity with current state-of-the-art sources. The usability of the current system is also limited by the experimental time, but decreasing the jet diameter to 30 μm will increase the liquid-metal-jet operating time $\sim 6\times$, making the first imaging applications possible.

6 Power Scaling

The interesting feature of this new anode technology is its scalability to high-brightness operation. Looking at the equations in Sec. 2.2 it is clear that the attainable brightness is a linear function of jet speed and independent of the jet diameter. As an example, consider a 600-m/s, 30-μm-diam liquid Sn [$\rho = 7.0 \times 10^3$ kg/m^3, $c_p = 230$ J/(kg K), $E_{vap} = 2.45 \times 10^6$ J/kg, $\Delta T \approx 2000$ K] jet. The power required for vaporization is 9 kW, corresponding to an electron-beam power density of 12 MW/mm^2. This is $\sim 100\times$ higher than the effective electron-beam power density in current sources. When considering the scalability and ultimate limit of this new anode concept several different aspects must be considered.

6.1 *Line-Focus Principle and the Liquid-Metal-Jet Anode*

As described in Sec. 1.1, the effective electron-beam power density in conventional anodes can be increased by using the line-focus principle. For the liquid-metal-jet anode, the situation is somewhat more complicated. A line focus along the jet axis does not increase the brightness, since the total power required for vaporization does not change. Only by using a line focus perpendicular to the jet can the brightness be increased, since the power remains constant but the effective area decreases. However, viewing a circular jet from the side will never decrease the apparent source size more than to half the jet diameter, so the only way to improve brightness significantly is to use a flat jet. Taking this into account, the maximum effective power density becomes

$$\frac{P}{A_{\text{effective}}} = \frac{w}{t}(2p\rho)^{1/2}(\Delta T c_p + E_{\text{vap}}), \tag{7}$$

where we now assume a flat jet with thickness t and width w matched to an electron beam with height t and width w viewed at an angle to produce an effective spot size of $t \times t$. The gain factor here is basically the same as in the rotating-anode case, and with the same examples as before but with a 30×300 μm^2 liquid-tin jet the effective power density would now be $\sim 1000\times$ compared to current technology.

6.2 *High-Speed Liquid-Metal Jets in Vacuum*

The hydrodynamics of the liquid-metal jet will be only briefly described here to show the feasibility of stable, continuous high-speed liquid-metal jets in vacuum, as required

in the power scaling examples. The hydrodynamic state of liquid jets is normally characterized by the use of Reynolds (Re) and Ohnesorge (Oh) number. The jet parameters in the proof-of-principle experiment ($d=75\ \mu$m, $\eta=2.1\times10^{-3}$ Ns/m^2, $\sigma=0.51$ N/m, $\rho=8.0\times10^3$ kg/m^3, $v=60$ m/s) result in Re$=1.7\times10^4$ and Oh$=3.8\times10^{-3}$. In a conventional Ohnesorge diagram,[20] this places the jet in the transition region between laminar and fully turbulent flow. However, as is clear from Fig. 5, the current jet exhibits Rayleigh drop breakup, characteristic of laminar jets. This is believed to be due to the vacuum environment and the resulting lack of air friction forces. It is therefore believed, as supported by other investigations,[21] that the normal spray limit does not apply when operating in a vacuum environment and that it will not limit the attainable speed for a collimated jet. Current water-jet cutting technology operates well into the spray region with a sufficiently stable and coherent jet.[22] Due to its higher density, the liquid-metal jet will require a very high backing pressure ($\sim10^4$ bar), on the limit of what is commercially available. The large mass transport will also require on-line recycling of the target material. A more detailed discussion on high-speed liquid-metal jets in vacuum is in preparation.[23]

6.3 *High-Power-Density Electron Beams*

The preceding power-scaling examples require that a correspondingly intense electron-beam focus can be achieved. This requires a 110 kW ($p\approx3.5\times10^{-8}$ AV$^{-3/2}$ for a 100-kV beam) beam to be focused to $30\times300\ \mu$m^2. This appears possible, although the perpendicular line focus will require careful electronoptics design to achieve the required combination of focal size and acceptable working distance, since the space-charge self-repulsion at this perveance will double the beam diameter in $\sim$75 beam diameters.[19] However, electron beams with similar perveance but with larger working distances and focal spots are found in electron-beam welding technology (see, e.g., Ref. 24).

6.4 *Liquid-Metal-Jet/e-Beam Interaction and Vacuum Issues*

The preceding brightness calculations are valid only if the entire volume is heated. Since the penetration depth of kilo-electron-volt electrons in metals is limited to a few micrometers, this is a problem since the thermal conduction is negligible on the time scale of the electron-focus transit (50 ns with a 600-m/s jet and a 30-μm focus). This can be alleviated by either increasing the beam energy so the penetration depth matches the jet diameter, or by using multiple electron beams for a more uniform heating. In terms of brightness, the penetration depth is not a major problem since the brightness does not scale with absolute dimensions. However, for high average power, where a large volume must be heated, it becomes a problem.

The major uncertainty in the power scaling of the liquid-metal-jet anode lies in the electron beam interaction with the metal jet. The preceding calculations assume that the entire liquid jet is evaporated during the electron-beam transit time. However, given a 50-ns transit time, it is unclear how the jet will react to this rapid heating and how the evaporation will occur. The average thermal speed of evaporated atoms, at the boiling point, is comparable with the jet speed and the jet should therefore expand into a cone after the electron-beam interaction point. This means that broadening of the focal spot due to evaporation should be limited. Furthermore, it should be possible to collect the jet plume in some sort of differential pumping scheme to maintain a decent vacuum around the interaction point. For cathode lifetime reasons, the acceleration part of the electron gun requires a good vacuum, but at the interaction point the demand is moderate as it is governed by the x-ray absorption and electron beam transport. This vacuum difference could also be maintained by a differential pumping scheme, or possibly by a plasma window.[25]

If the vacuum problem associated with heating the entire jet volume to evaporation can be managed, the actual power-load limit may be even further increased since applying even more power will not drastically increase the problem. On the other hand, assume that the evaporation problem can not be overcome and the heating must be reduced below the boiling point. Then the achievable brightness is reduced to $\sim$10% (depending on tolerable vacuum load) of the numbers mentioned throughout this paper for Sn, as this is the contribution from heating. Even with this drastic reduction, the possible gain in brightness of the new anode concept compared to existing technology will be $\sim100\times$.

7 Conclusions

We reported on the progress of a new liquid-metal-jet anode electron-impact x-ray tube. Initial calculations showed that this source concept could potentially increase the brightness in compact electron-impact x-ray sources $>100\times$ compared to current state-of-the-art technology. A first, successful, proof-of-principle experiment at low power was performed to demonstrate the feasibility of the concept although the ultimate brightness still remains to be proven experimentally. This could potentially result in a brightness on the order of 10^{13} photons/(s mm^2 mrad^2) in the 25-keV Sn K_α-line. For comparison, bending-magnet radiation from modern 6 to 8-GeV synchrotron sources typically have a brightness of the order of 10^{15} photons/(s mm^2 mrad^2 0.1% bandwidth). However, the large size (typical diameter >100 m) and expense of such machines will always limit their applicability to special cases, while the compact sources have potential to find widespread use in the small to medium-scale laboratory or clinic. Since several important applications of compact sources, such as mammography, angiography, protein crystallography, and phase imaging, stand to gain from an increase in brightness, we feel that the initial results presented here warrant further work to investigate this new anode concept.

Acknowledgments

The authors gratefully acknowledge the work by Thomas Koch on electron-beam simulations and Joseph Nordgren for discussions. This work has been supported by the Swedish Agency for Innovation Systems and the Swedish Research Council.

References

1. J. Beutel, H. L. Kundel, and R. L. Van Metter, *Handbook of Medical Imaging*, Vol. 1, SPIE Optical Engineering Press, Bellingham, WA (2000).
2. E. Krestel, *Imaging Systems for Medical Diagnostics*, Siemens, Berlin (1990).
3. J. S. Price, "Review of challenges in medical diagnostic x-ray sources," *Proc. SPIE* **4502**, 1–9 (2001).
4. J. Freudenberger, E. Hell, and W. Knüpfer, "Perspectives on medical x-ray imaging," *Nucl. Instrum. Methods Phys. Res. A* **466**(1), 99–104 (2001).
5. C. Giacovazzo, *Fundamentals of Chrystollagraphy*, Oxford University Press, New York (1992).
6. R. Fitzgerald, "Phase-sensitive x-ray imaging," *Phys. Today* **53**(7), 23–26 (2000).
7. B. K. Agarwal, *X-Ray Spectroscopy*, Springer-Verlag, New York (1991).
8. Thermo Kevex micro-focus source PXS5-926EA (http://www.kevex.com).
9. O. Hemberg, M. Otendal, and H. M. Hertz, "Liquid-metal-jet anode electron-impact x-ray source," *Appl. Phys. Lett.* **83**(7), 1483–1485 (2003).
10. L. Rymell and H. M. Hertz, "Droplet target for low-debris laser-plasma soft x-ray generation," *Opt. Commun.* **103**, 105–110 (1993).
11. L. Rymell, M. Berglund, and H. M. Hertz, "Debris-free single-line laser-plasma x-ray source for microscopy," *Appl. Phys. Lett.* **66**, 2625–2627 (1995).
12. B. A. M. Hansson, L. Rymell, M. Berglund, O. Hemberg, E. Janin, S. Mosesson, J. Thoresen, and H. M. Hertz, "Liquid-xenon-jet laser-plasma source for EUV lithography," *Proc. SPIE* **4506**, 1–8 (2001).
13. G. Korn, A. Thoss, H. Stiel, U. Vogt, M. Richardson, T. Elsaesser, and M. Faubel, "Ultrashort 1-kHz laser plasma hard x-ray source," *Opt. Lett.* **27**, 866–868 (2002).
14. B. Buijsse, "keV-electron-based table-top soft x-ray source," *Proc. SPIE* **4502**, 74–81 (2001).
15. R. K. Smither, K. Robert, G. S. Knapp, E. M. Westbrook, and G. A. Forster, "High intensity x-ray source using liquid gallium target," U.S. Patent No. 4,953,191, filed July 24, 1989.
16. M. Schuster, "X-ray generator," U.S. Patent No. 5,052,034, filed October 29, 1990.
17. B. R. David, H. Barschdorf, V. Doormann, R. Eckart, G. Harding, J. Schlomka, A. Thran, P. Bachmann, and P. Flisikowski, "Liquid metal anode x-ray tube," *Proc. SPIE* **5196**, 432–443 (2003).
18. J. F. Douglas, J. M. Gasiorek, and J. A. Swaffield, *Fluid Mechanics*, 3rd ed., John Wiley & Sons, New York (1995).
19. M. Sedlaček, *Electron Physics of Vacuum and Gaseous Devices*, John Wiley & Sons, New York (1996).
20. A. H. Lefebvre, *Atomization and Sprays*, Hemisphere Publishing Corp., New York (1989).
21. R. W. Fenn III and S. Middleman, "Newtonian jet stability: the role of air resistance," *AIChE J.* **15**(3), 379 (1969).
22. D. A. Summers, *Waterjetting Technology*, Routledge, New York (1995).
23. M. Otendal, O. Hemberg, and H. M. Hertz, "Microscopic high-speed liquid-metal jets in vacuum," submitted to Phys. Fluids.
24. Steigerwald EBOPULS G 120 PMS (http://www.steigerwald-eb.de).
25. A. Hershcovitch, "A plasma window for transmission of particle beams and radiation from vacuum to atmosphere for various applications," *Phys. Plasmas* **5**(5), 2130 (1998).

Oscar Hemberg received his MSc degree in engineering physics from the Royal Institute of Technology, Stockholm, Sweden, in 1999 and joined the Biomedical and X-Ray Physics Group where his initial research was in the field of laser-produced plasmas for soft x-ray and EUV generation. In 2000 Mr. Hemberg cofounded Innolite AB, an EUV source company. His current research interest is compact, high-brightness, electron-impact x-ray sources based on liquid-metal-jet anodes. Mr. Hemberg's research has resulted in several scientific articles and patents.

Mikael Otendal received his MSc degree in engineering physics from Lund University, Sweden, in 2001 and is currently a PhD student at the Royal Institute of Technology, Stockholm, Sweden. Within the high-brightness x-ray source research project, Mr. Otendal's special interest is in high-speed liquid-metal jets in vacuum.

Hans M. Hertz received his PhD degree in physics in 1988 from Lund University, Sweden, and did his postdoctoral work at Stanford University. Since 1997 he has been a full professor with the Royal Institute of Technology, Stockholm. His present research interests are compact laser-plasma soft x-ray sources, x-ray microscopy, x-ray optics, hard x-ray sources, and biomedical applications of x rays as well as of ultrasonic radiation pressure. His recent achievements include the first liquid-jet-target laser-plasma sources for soft x-ray and extreme UV generation, the first liquid-metal-jet anode hard x-ray source, and the first compact laser-plasma soft x-ray microscope with suboptical resolution. Hertz is a member of several professional societies, has published more than 70 scientific papers, and holds several patents.